PHOTONICS Research

Extremely regular periodic surface structures in a large area efficiently induced on silicon by temporally shaped femtosecond laser

Yuchan Zhang,[1] Qilin Jiang,[1] Kaiqiang Cao,[1] Tianqi Chen,[1] Ke Cheng,[1] Shian Zhang,[1] Donghai Feng,[1] Tianqing Jia,[1,2,*] Zhenrong Sun,[1] and Jianrong Qiu[3]

[1]State Key Laboratory of Precision Spectroscopy, School of Physics and Materials Science, East China Normal University, Shanghai 200062, China
[2]Collaborative Innovation Center of Extreme Optics, Shanxi University, Taiyuan 030006, China
[3]State Key Laboratory of Optical Instrumentation, Zhejiang University, Hangzhou 310027, China
*Corresponding author: tqjia@phy.ecnu.edu.cn

Received 11 January 2021; revised 2 March 2021; accepted 4 March 2021; posted 8 March 2021 (Doc. ID 418937); published 30 April 2021

Femtosecond laser-induced periodic surface structures (LIPSS) have several applications in surface structuring and functionalization. Three major challenges exist in the fabrication of regular and uniform LIPSS: enhancing the periodic energy deposition, reducing the residual heat, and avoiding the deposited debris. Herein, we fabricate an extremely regular low-spatial-frequency LIPSS (LSFL) on a silicon surface by a temporally shaped femtosecond laser. Based on a $4f$ configuration zero-dispersion pulse shaping system, a Fourier transform limit (FTL) pulse is shaped into a pulse train with varying intervals in the range of 0.25–16.2 ps using periodic π-phase step modulation. Under the irradiation of the shaped pulse with an interval of 16.2 ps, extremely regular LSFLs are efficiently fabricated on silicon. The scan velocity for fabricating regular LSFL is 2.3 times faster, while the LSFL depth is 2 times deeper, and the diffraction efficiency is 3 times higher than those of LSFL using the FTL pulse. The formation mechanisms of regular LSFL have been studied experimentally and theoretically. The results show that the temporally shaped pulse enhances the excitation of surface plasmon polaritons and the periodic energy deposition while reducing the residual thermal effects and avoiding the deposition of the ejected debris, eventually resulting in regular and deeper LSFL on the silicon surface.

https://doi.org/10.1364/PRJ.418937

1. INTRODUCTION

Femtosecond laser-induced periodic surface structures (LIPSS) have been widely studied over the last 20 years [1–4]. These periodic nanostructures efficiently modify the properties of materials and have many applications in surface coloring [5,6], large-area grating [7,8], birefringence optical elements [9], data storage [10], and surface wettability [11,12]. In general, three main characteristics are considered for evaluating the quality of LIPSS: uniformity, depth, and orientation, which have a significant influence on their functions.

Numerous experimental and theoretical studies investigated the formation mechanism of low-spatial-frequency LIPSS (LSFL) with a spatial period $\Lambda > \lambda/2$, where λ is the laser wavelength [1,2,4,13,14]. For semiconductors and metals, the orientation of LSFL was usually perpendicular to the incident laser polarization, which was widely accepted as a result of the laser energy periodic distribution induced by surface plasmon polaritons (SPPs) [1,14]. Therefore, the control and enhancement of SPPs is a fundamental challenge for obtaining regular LSFL. Jiang *et al.* [15] attempted to control the localized transient electron dynamics by temporally or spatially shaping femtosecond pulses and further attempted to modify the properties of transient materials. Jalil *et al.* [16] fabricated uniform LSFL on nickel using two collinear femtosecond lasers at various temporal delays and attributed the regular LSFL to the reduction in the propagation length of SPP. The research to effectively regulate and enhance SPPs is still in progress.

During LSFL formation on the semiconductor and metal surfaces induced by Fourier transform limit (FTL) laser pulses, a part of the ejected ablation plume deposited on the surface and formed a massive amount of debris [17]. Yang *et al.* [18] experimentally demonstrated the generation and erasure of LIPSS on a Si surface under irradiation with a single femtosecond laser pulse, which was due to the opposition between periodic surface structuring and surface smoothing associated with surface melting. Cheng *et al.* [19,20] clearly demonstrated the transient LSFL at a delay time of 150–400 ps on gold, silver, and nickel. These ripples were totally/partly submerged after

solidification owing to the residual thermal effect. The deposited debris and the residual heat significantly affected the SPP excitation, propagation, and light field distribution during the subsequent laser irradiation, resulting in significant distortions and bifurcations on LIPSS.

The enhancement of the strength of SPPs along with reducing the ablation debris and residual heat so as to fabricate LSFL with a high homogeneity and depth is a significant and fundamental research topic. In this paper, based on a $4f$ configuration zero-dispersion pulse shaping system, an FTL pulse is shaped into a pulse train using periodic π-phase step modulation. The LSFL fabricated by a shaped pulse of 16.2 ps is very straight and regular, with much less ablation debris. The LSFL depth fabricated by a shaped pulse of 16.2 ps is much larger than that of the FTL pulse, and the scanning velocity is also much faster. Large-area extremely regular LSFLs are fabricated by direct writing with a shaped pulse of 16.2 ps. The diffraction spectra are 36–20 nm wide in the range of 400–700 nm, and the diffraction efficiency is 3 times higher than that of the FTL pulse. The fabricated pattern of "Chinese knot" on the Si surface shows a vivid structural color. The formation mechanisms of regular LSFL were studied in detail through investigating the formation processes by changing the laser fluences and scanning velocity, and by theoretical calculation with the two-temperature-Drude model (TTM–Drude model).

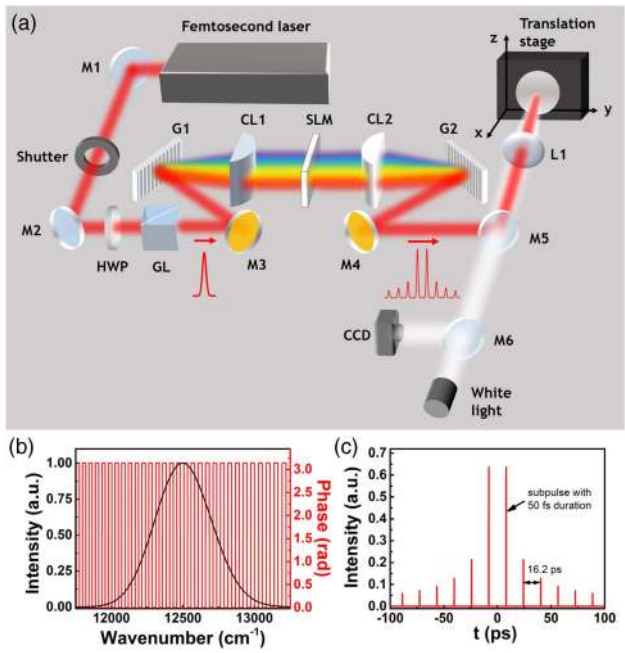

Fig. 1. (a) Experimental setup used for processing LSFL on silicon with a temporally shaped femtosecond laser. (b) Periodic π-phase step modulation applied to the laser spectrum. (c) Temporal intensity profile of the shaped pulse of 16.2 ps with a modulation period of 4.5 cm^{-1}.

2. EXPERIMENTAL SETUP AND THE PROPOSED MODEL

A. Experimental Setup

A Ti:sapphire laser system output femtosecond laser pulses with a duration of 50 fs, a center wavelength of 800 nm, and a repetition rate of 1000 Hz. A half-wave plate (HWP) and a Glan prism (GL) were used to adjust the laser pulse energy. As shown in Fig. 1(a), the laser travels through a $4f$ configuration zero-dispersion pulse shaping system. The temporally shaped pulse is focused on the Si surface by a lens with a focal length of 200 mm. The diameter of the laser spot size at focus is 36 μm, measured by laser ablation method [21]. The Si wafer is translated using a three-axis translation stage with an accuracy of 1 μm. A white light source and a charge-coupled device (CCD) are used for monitoring the laser fabrication process.

The $4f$ configuration zero-dispersion pulse shaping system consists of a pair of diffraction gratings with 1200 lines/mm (G1 and G2) and a pair of convex cylindrical lenses with a 400 mm focal length (CL1 and CL2) [22,23]. A one-dimensional programmable liquid crystal spatial light modulator (LC-SLM, SLM-S320d, Jenoptik) is placed at the Fourier plane to modulate the spectral phase. As shown in Fig. 1(b), a periodic π-phase step modulation is applied to the laser spectrum to generate femtosecond laser pulse trains [24]. Figure 1(c) shows the temporal intensity profile of a shaped pulse with a modulation period of 4.5 cm^{-1}, while the interval between two adjacent sub-pulses is 16.2 ps, which can be varied by changing the modulation period. The two primary sub-pulses exhibit a maximum normalized peak intensity of 0.63, and the intensities of the three outward sub-pulses are 0.21, 0.13, and 0.09, respectively. In this paper, the initial femtosecond laser pulses are denoted by the FTL pulse, and the pulse trains are denoted by the corresponding interval, such as a shaped pulse of 16.2 ps. The interval of the sub-pulses can be adjusted in a range of 0.25–16.2 ps.

The sample was a commercial 0.5 mm thick undoped Si wafer (100) (MTI-group, China). The surface was optically polished with a roughness of <1 nm. The morphology and depth of the LSFL were measured using a scanning electron microscope (SEM) (S-4800, Hitachi, Japan) and a confocal microscope (Smartproof 5 Widefield Confocal Microscope, Zeiss, Germany), respectively. A fiber optical spectrometer (Ocean-2000, Ocean Optics, USA) was utilized to measure the diffraction spectrum of the larger-area LSFL. Structural colors ranging from red to purple were captured by a camera at different angles.

B. Proposed Model of Shaped Pulse Laser-Induced Regular and Deep LSFL

The ultrafast imaging results demonstrated that the transient LSFL began to form on the sample surface after several to tens of picoseconds (ps) after the laser irradiated on the Si surface [25]. Therefore, there are transient LSFLs on Si surfaces after irradiation by the two main sub-pulses of 16.2 ps as shown in Fig. 2. When the subsequent sub-pulse reaches the surface, the surface changes to a metal-like state and effectively supports the excitation of SPPs [1,25]. The transient gratings induced by the previous sub-pulses enhance the excitation of SPPs and the periodic laser field [1]. The substrate in the surface region remains at very high temperature when the subsequent sub-pulse reaches the Si surface. Part of the material is further excited and ejected from the surface, and it removes the

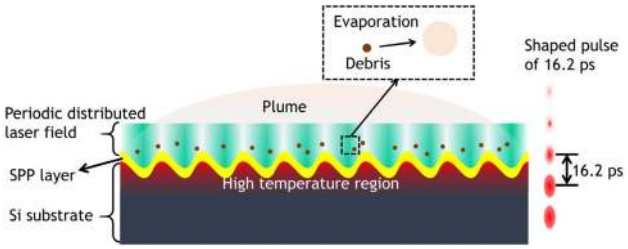

Fig. 2. Schematic diagram of shaped pulse laser-induced regular and deep LSFL. The red area in the Si substrate presents the high temperature region when the sub-pulse reaches the surface.

deposited heat (ablation-cooling effect) [26]. The ejected materials by the previous sub-pulse, including plume and debris, will be further excited by the subsequent sub-pulses, and the debris is further ionized and vaporized into aerosol, resulting in less deposited particles [17,18]. The SPPs and the periodic laser energy deposition are enhanced, and the residual heat is reduced. Therefore, regular and deep LSFL can be induced on a Si surface by the shaped pulse of 16.2 ps.

3. EXPERIMENTAL RESULTS

A. Large-Area Extremely Regular LSFL Fabricated by Laser Direct Writing with a Shaped Pulse of 16.2 ps

Figure 3 shows a large area of extremely regular LSFL fabricated by a temporally shaped pulse of 16.2 ps through laser direct writing in parallel lines. The laser fluence and scan velocity were 0.70 J/cm^2 and 8.0 mm/s, respectively, and the distance between two adjacent lines was 21 μm. Figure 3(a) shows the SEM image having the maximum available size, which is filled with extremely homogeneous LSFL. Figure 3(b) shows a magnified SEM image with an area of 100 μm × 70 μm. In particular, the LSFLs are completely parallel to the two edges of the SEM image within such a large size, indicating that the LSFLs are extremely straight and regular. Figures 3(c) and 3(d) depict a further enlarged view, clearly demonstrating that each ripple is completely straight and uniform. Figure 3(f) is a 2D fast Fourier transform (FFT) image of Fig. 3(b). The FFT peak along the x axis is at 1.289 ± 0.008 μm^{-1}, corresponding to a period of 774 ± 5 nm as shown in Fig. 3(g). Such a small fluctuation of period further shows that the LSFL is very uniform and straight. Due to the limitation of the size of the optical table, the interval of sub-pulses cannot be increased any longer. We estimate that the optimum interval of the sub-pulse is in a range of 30–300 ps according to the reports of ultrafast imaging of transient LSFL and ablation cooling effects [19,20,25,26]. Huang *et al.* precisely manipulated the laser-material interaction process to generate amorphous-crystalline LIPSS, which was mainly accompanied by phase changing of crystalline Si with almost no material removal. The periodic surface structures fabricated by this method were very regular. However, the window of laser fluence was very narrow, and processing efficiency was very low [17].

Figure 3(e) shows an SEM image of the cross section of the LSFL cut with a focused ion beam (FIB). The edges of the LSFL are significantly straight. The grooves are very regular and consistent with a depth of 97.6 ± 2 nm. The white stripe is a Pt film coated before FIB cutting.

The optical characterization measurement was used to study the diffractive properties of large-area LSFL as shown in Fig. 4(a). A wide-spectrum light source (400–2200 nm, tungsten halogen lamp) was vertically incident on the sample, and a fiber spectrometer was mounted on a 3D rotational stage to obtain the diffraction spectra at different angles. The screen/CCD can replace the fiber spectrometer to observe the diffraction patterns/structural colors, respectively.

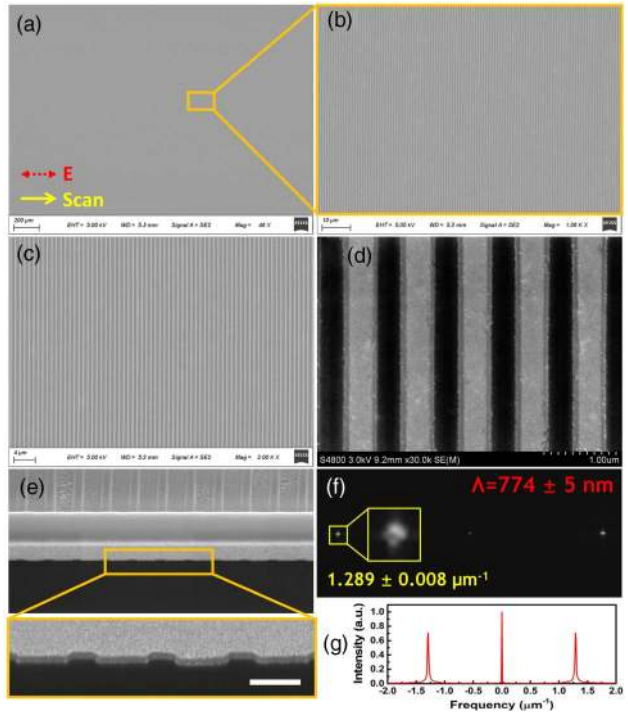

Fig. 3. (a)–(d) SEM images of LSFL fabricated by shaped pulse of 16.2 ps through laser direct writing in parallel lines. (e) SEM image of the cross section of the LSFL. (f) 2D-FFT image of (b). (g) Spectrum of the FFT along the x axis. The scale bar in (e) is 500 nm long. The dash arrow in (a) presents the laser polarization, and the solid arrow presents the scan direction.

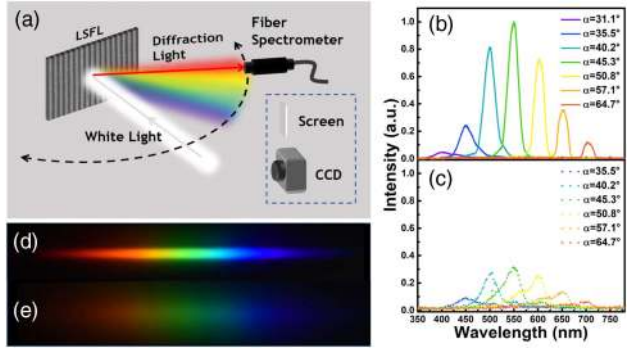

Fig. 4. (a) Optical characterization measurement for testing the diffractive properties of large-area LSFL. The diffraction spectra from the LSFL fabricated (b) by shaped pulse of 16.2 ps and (c) by FTL pulse. The orderly multicolor diffraction pattern from the LSFL fabricated (d) by shaped pulse of 16.2 ps and (e) by FTL pulse.

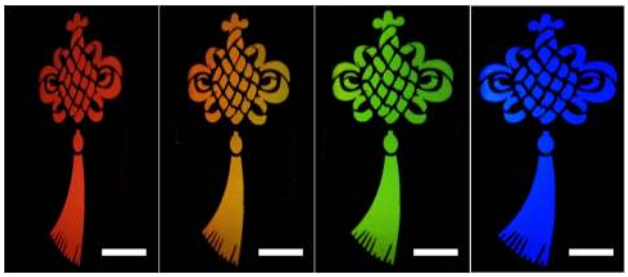

Fig. 5. Structural colors of "Chinese knot" pattern made up of LSFL fabricated by shaped pulse of 16.2 ps on Si surface. The white scale bars are 5 mm long.

The large-area LSFLs fabricated by the shaped pulse of 16.2 ps ($F = 0.70$ J/cm^2, $v_{scan} = 8$ mm/s) and FTL pulse ($F = 0.48$ J/cm^2, $v_{scan} = 8$ mm/s) with a line space of 21 μm were mounted on the same stage and measured in sequence. The diffraction spectra at different angles are depicted in Figs. 4(b) and 4(c), respectively. The diffraction spectra can be characterized by the diffraction grating equation as $d \sin\alpha = m\lambda$, where m is the diffraction order, d is the grating constant (LSFL period), and α is the diffraction angle. For the LSFL fabricated by a shaped pulse of 16.2 ps, the FWHM values of the diffraction peaks at 450, 500, 550, 600, and 650 nm are only 36, 28, 25, 22 and 20 nm, respectively. Moreover, the diffractive efficiency is 3 times larger than that using the FTL pulse. Figure 4(d) presents the orderly multicolor diffraction patterns from the LSFL fabricated by the shaped pulse of 16.2 ps. The colors range from red to purple at different diffraction angles, which are obviously brighter, clearly distinguished, and much narrower than those from the FTL pulse [Fig. 4(e)]. These results further demonstrate that the quality of the LSFL fabricated by the shaped pulse of 16.2 ps is significantly better than that by the FTL pulse.

Owing to the strong absorption and scattering of blue light by the Si surface, the structural color of blue is usually dark and appears to be blue-green. A pattern of "Chinese knot" with a size of 20 mm × 30 mm is processed by laser direct writing of the shaped pulse of 16.2 ps. Figure 5 presents the red, yellow, green, and blue structural colors, which are all very homogeneous and bright. The bright blue color further confirms that the temporally shaped pulse is capable of producing any desirable pattern with significantly regular LSFL.

B. LSFL Fabricated by a Shaped Pulse of 16.2 ps and FTL Pulse

1. Window of the Laser Fluence for Fabricating Regular LSFL at a Different Scan Velocity

Laser fluence and scan velocity are two key parameters in femtosecond laser processing of uniform and regular LSFL. The homogeneous alternating amorphous-crystalline LSFL was induced by an FTL pulse under a low laser fluence, and the scan velocity was usually less than 2.0 mm/s under 1 kHz repetition [17], which indicates a low fabricating efficiency. In order to increase the scan velocity and LSFL depth, it is necessary to increase the laser fluence. However, this will partially enhance laser ablation and cause massive debris and surface defects. Debris and surface defects substantially affect the generation of SPPs and the distribution of the light field of subsequent laser pulses, resulting in curved and cracked LSFL, even partially smoothed by the molten layer [18].

Figure 6(a) presents the laser fluence windows for fabricating spaced, regular, and partly damaged LSFL on the Si surface at different scan velocities. The upper and lower areas demonstrate the results obtained by using the shaped pulse of 16.2 ps and the FTL pulse, respectively. When the scan velocity is 5.0 mm/s, the laser fluence for the regular LSFL fabricated by the FTL pulse is in a range of 0.40–0.44 J/cm^2. At this scan velocity, the maximum window is 0.04 J/cm^2. For the shaped pulse of 16.2 ps, the fluence window is in the range of 0.67–0.72 J/cm^2. The window width is 0.05 J/cm^2, which is slightly larger than that of the FTL pulse at the same scan velocity. At this scan velocity, regular LSFLs are fabricated by the two types of laser pulses as shown in the SEM images in Figs. 6(s2) and 6(f2).

When the scan velocity increases to ≥8.0 mm/s, the overlapped pulse number is too low to support the formation of a regular LSFL fabricated by an FTL pulse. When the laser fluence is less than 0.46 J/cm^2, only spaced and curved ripples are formed as shown in Fig. 6(f4). When the laser fluence is

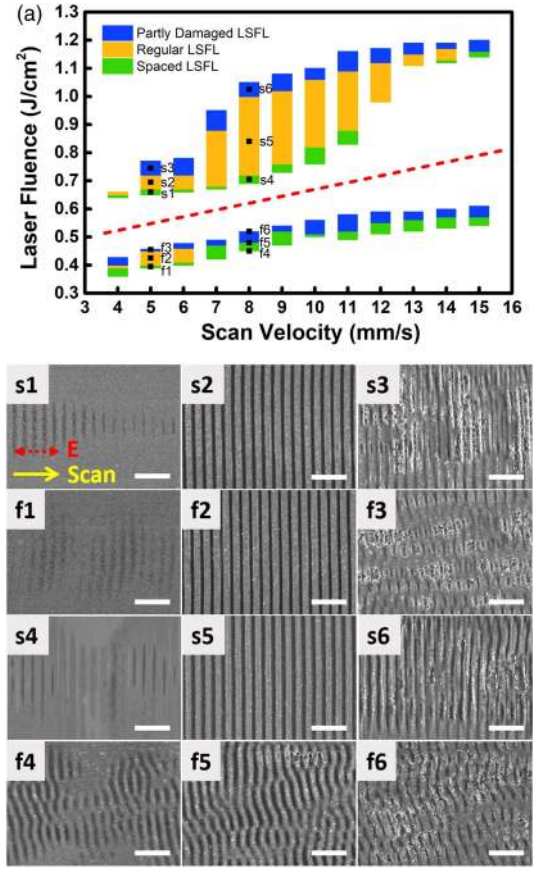

Fig. 6. (a) At different scan velocity, the laser fluence windows for fabricating spaced (green), regular (orange), and partly damaged (blue) LSFLs by shaped pulse of 16.2 ps (the upper area) and by FTL pulse (the lower area). The SEM images (s1)–(s6) and (f1)–(f6) are the corresponding LSFLs of the marked points in (a). The dash arrow in (s1) presents the laser polarization, and the solid arrow presents the scan direction. The scale bars have a length of 3 μm.

0.48 J/cm^2, the spaced ripples start to connect with each other but are much curved with many bifurcations because of debris and residual thermal effects as shown in Figs. 6(f5) and 6(f6).

Because each shaped pulse contains many sub-pulses, when the scan velocity gradually increases, the laser fluence window of the regular LSFL becomes larger, which is very different from the FTL pulse. When the scan velocity increases to 8.0 mm/s, regular LSFLs are fabricated in the range of 0.72–1.00 J/cm^2. The maximum window was 0.28 J/cm^2, which is 7 times larger than the maximal window of the FTL pulse (0.04 J/cm^2 at a scan velocity of 5 mm/s). Figure 6(s5) depicts a very regular LSFL with a period of 770 nm for a laser fluence $F =$ 0.84 J/cm^2. When the laser fluence is 0.68 J/cm^2, the spaced LSFLs are still very straight without any debris as shown in Fig. 6(s4). When the laser fluence is larger than 1.00 J/cm^2, the LSFL with a part of the damaged area is still in a good arrangement as shown in Fig. 6(s6). When the scan velocity increased to 12 mm/s, the laser fluence window of the regular LSFL is still as large as 0.14 J/cm^2. Under the irradiation of the temporally shaped pulse of 16.2 ps, the laser fluence window of regular LSFL is larger and the scan velocity is faster, which indicates that the temporally shaped pulse is a good method to achieve high efficiency and stability in fabricating regular LSFLs.

2. Groove Depth of LSFL

Improving the depth of LSFL is an important factor for improving the diffraction efficiency, structural colors, and birefringence effect [7,27]. Figures 7(a) and 7(b) demonstrate the confocal microscopy images of the most regular LSFL fabricated by the FTL pulse [Fig. 6(f2)] and by the shaped pulse of 16.2 ps [Fig. 6(s2)]. The two SEM images show similar LSFL, but the depth is significantly different. Figures 7(c) and 7(d) are the 2D plots of the cross sections along the yellow arrows in Figs. 7(a) and 7(b), respectively. For the FTL pulse, the LSFL depth at the center of the ablation trace is 57 ± 6 nm. The groove depth has a fluctuation of 6 nm, which is approximately 10.5% of the average depth of 57 nm. For the LSFL fabricated by the shaped pulse of 16.2 ps, the depth is 103 ± 3 nm, that is, 1.8 times deeper than the ripples fabricated by the FTL pulse. Moreover, the groove depth is more uniform. The fluctuation is only 3 nm, which is approximately 2.9% of the average depth of 103 nm. Figure 7(e) presents the average depth from the edges to the center of the ablation trace. The width of the ripples deeper than 100 nm is 14 μm for the shaped pulse, while it is only 10 μm wide for the ripples deeper than 50 nm for the FTL pulse. Furthermore, the bottom of the ablation trace by the shaped pulse is flatter. In summary, even when compared with the best LSFL fabricated by the FTL pulse, the LSFL fabricated by the shaped pulses of 16.2 ps is much deeper and more uniform, and the bottom of the ablation trace is wider and flatter.

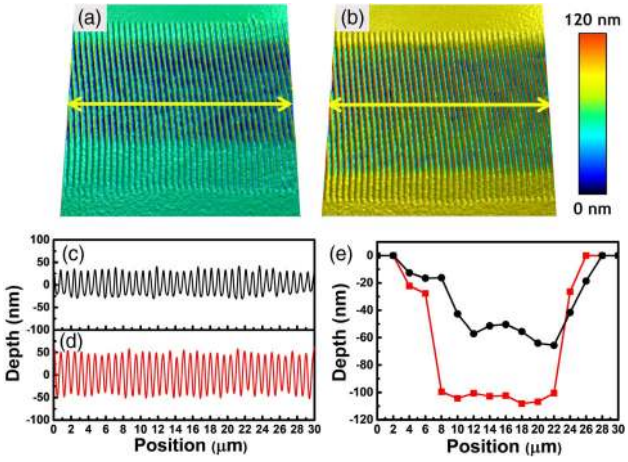

Fig. 7. Confocal microscopy images of the regular LSFL fabricated by (a) FTL pulse ($F = 0.43$ J/cm^2) and (b) shaped pulse of 16.2 ps ($F = 0.69$ J/cm^2). The scan velocity is 5.0 mm/s. (c) and (d) 2D plots of the cross sections along the yellow arrows in (a) and (b), respectively. (e) Average depth of the LSFL along the cross section perpendicular to the ablation trace.

Table 1. DSOA of the Regular Ripples and Partly Damaged Ripples in Fig. 6

LSFL	s2	s3	s5	s6
DSOA	3.7°	6.7°	2.5°	5.8°
LSFL	f2	f3	f5	f6
DSOA	4.0°	11.5°	17.5°	22.5°

3. Orientation of LSFL

To characterize the uniformity of LSFL, the local orientations of the structures in Figs. 6(s2),6(s3),6(f2),6(f3) and 6(s5), 6(s6), 6(f5), 6(f6) are analyzed through an open software "ImageJ" with the "OrientationJ" plugin [28] as shown in Table 1. The divergence of the structure orientation angle (DSOA) is the half-width at half-maximum value of the distribution. The DSOA of the regular LSFL in Fig. 6(s2) is 3.7°, which is slightly smaller than that of Fig. 6(f2). However, for the partly damaged LSFL, the DSOA of Fig. 6(s3) is only 6.7°, which is significantly less than that of Fig. 6(f3). These results indicate that the partly damaged ripples fabricated by the shaped pulse of 16.2 ps are considerably more homogeneous and regular than those fabricated by the FTL pulse at lower scan velocities. When the scanning velocity is increased to 8.0 mm/s, the DSOA of the regular ripples fabricated by the shaped pulse of 16.2 ps surprisingly drops to 2.5°, which is even smaller than that of the alternating amorphous-crystalline LSFL [7]. These results further demonstrate that the LSFLs induced by the shaped pulse of 16.2 ps are much more homogeneous and straighter than that of the FTL pulse, especially for high-speed fabrication.

C. Mechanisms of the Regular LSFL Fabricated by a Temporally Shaped Laser Pulse

To investigate the formation mechanism of the regular LSFL induced by the shaped pulse of 16.2 ps, the ripples fabricated at different scanning velocities under the irradiation of an FTL pulse and the shaped pulse of 16.2 ps are studied in detail. The two-temperature model and Drude model (TTM–Drude model) were used to study the evolution of electron density, electron temperature, lattice temperature, and dielectric constant on the Si surface after irradiation with the shaped pulse of 16.2 ps or FTL pulse. The experimental and theoretical results elucidate the formation mechanisms of regular LSFL.

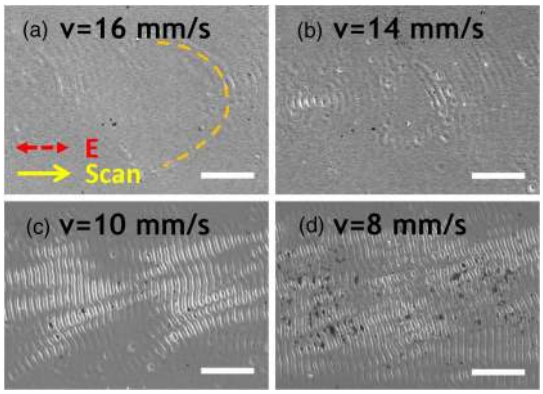

Fig. 8. SEM images of the surface nanostructures fabricated by FTL pulse at different scanning velocities of (a) 16 mm/s, (b) 14 mm/s, (c) 10 mm/s, and (d) 8 mm/s. The laser fluence was fixed at 0.54 J/cm^2. The dashed arrow presents the laser polarization, and the solid arrow presents the scanning direction. The scale bars are all 5 μm in length.

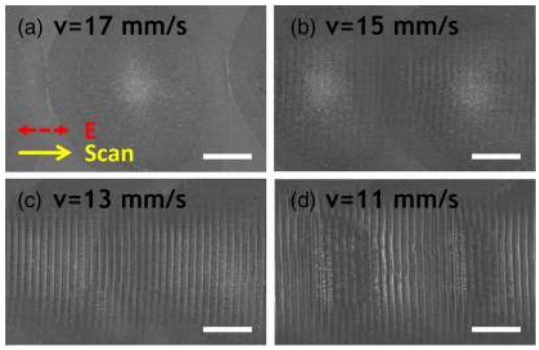

Fig. 9. SEM images of the surface nanostructures fabricated by shape pulse of 16.2 ps at different scanning velocities of (a) 17 mm/s, (b) 15 mm/s, (c) 13 mm/s, and (d) 11 mm/s. The laser fluence was fixed at 1.13 J/cm^2. The dashed arrow presents the laser polarization, and the solid arrow presents the scanning direction. The scale bars are all 5 μm long.

1. Formation of LSFL by FTL Pulse

Figure 8 presents the SEM images of the surface nanostructures fabricated by the FTL pulse at different scanning velocities, while the laser fluence was fixed at 0.54 J/cm^2. When the scan velocity was 16 mm/s, as shown in Fig. 8(a), the ablation spots are spaced at a distance of 16 μm. A few shallow, broken, and curved ripples appeared in the area near the outer edge of the ablation spot (orange dashed curve), which indicates that the edge of the ablation spot induced by the former pulse is the origin of SPPs during the irradiation of the next pulse [18]. In the neighboring area outside the edge of the ablation spot, the local laser fluence and the residual thermal effects are small, while the SPPs are strong; thus, the ripples remain. When the scan velocity decreased to 14 mm/s, more curved and broken ripples appeared, which are substantially disturbed by the deposited debris. When the scan velocity decreased to 10 mm/s, as shown in Fig. 8(c), more ripples grow deeper and longer, but there are still many bifurcations and ablative debris on themselves.

When the scan velocity further reduced to 8 mm/s, the curved LSFL filled in the ablation trace. A considerable amount of ablative materials are deposited on the surface. The ripples are partly melted and submerged owing to the thermal effect as shown in Fig. 8(d). When the scan velocity decreases to ≤6 mm/s, most of the ripples at the center of the ablation trace are submerged, owing to the thermal effect. The results show that, under the irradiation of the FTL pulse, the edge of the ablation spot is the origin of the SPPs, which induces curved and broken ripples. In addition, the deposited debris disturbs the excitation and propagation of SPPs [8], and the residual heat partly submerges the ripples. Therefore, the conditions to fabricate regular LSFLs under the irradiation of an FTL pulse are very strict.

2. Formation of LSFL by a Shaped Pulse of 16.2 ps

Figure 9 presents the ripples fabricated at different scanning velocities by the shaped pulse of 16.2 ps with a fixed laser fluence of 1.13 J/cm^2. When the scan velocity was 17 mm/s, as shown in Fig. 9(a), the adjacent ablation spots are separated, with a distance between centers of 17 μm. The edge of each ablation spot is very clear, and no ripples appear anywhere. When the scanning velocity was reduced to 15 mm/s, two adjacent ablation spots partially overlapped (approximately 2 μm) as shown in Fig. 9(b). Several shallow ripples with a period of 780 nm appeared on the ablation spots with an orientation perpendicular to the laser polarization. This result shows that SPPs also originate from the edge of the ablation spots, similar to the case of the FTL pulse.

It is worth noting that the LSFL appears in the entire ablation spot irradiated by the shaped pulse of 16.2 ps, rather than only in the vicinity outside the edge of the ablation spot by the FTL pulse. Moreover, these ripples are very straight and regular, considerably better than those obtained by the FTL pulse. The main influencing factors are as follows.

(1) Under the irradiation of an FTL pulse, the energy is mainly used to excite a plasma layer; only a small portion of the energy in the tail of the laser pulse is used to excite SPPs [1,25]. SPPs propagate simultaneously from the edge to the outside and inside of the ablation spots. Owing to the thermal effect caused by the higher local laser fluence, the LSFLs inside the ablation spots are submerged [25]. The LSFLs outside the ablation spots are reserved owing to the appropriate local laser fluence. However, irradiated by the shaped pulse of 16.2 ps, the first strongest sub-pulse excites the Si surface from the semiconductor to the metal-like state, which supports the excitation of SPPs [18,25]. The transient LSFLs induced by SPPs are the origin of the SPPs for the subsequent sub-pulses [1,25,29], which further enhance the excitation of the SPPs propagating perpendicularly to the laser polarization, resulting in the formation of straight and regular LSFL.

(2) The experimental results of ultrafast pump-probe imaging show that the Si surface begins to melt and ablate from a delay time of 1–30 ps after femtosecond laser irradiation [25,29]. The electron and lattice on the surface remain at a high temperature when the subsequent sub-pulses arrive at the surface irradiated by the shaped pulse of 16.2 ps. The subsequent sub-pulses further excite the high-temperature surface

and effectively ablate materials [26]. Under the irradiation of the shaped pulse of 16.2 ps, the residual thermal effect on the ablation spot is significantly reduced because of the "ablation cooling" effect [26], and the SPPs are considerably enhanced because of the "grating-light coupling" effect [1]; thus, the regular LSFLs are well preserved. This further explains the much deeper LSFL induced by the shaped pulse of 16.2 ps as shown in Fig. 6.

(3) As shown in Fig. 8, under the irradiation of the FTL pulse, a significant amount of ablative debris and particles were deposited on the surface, which substantially disturbed the formation of LSFL. In contrast, Fig. 9 shows that the Si surface is very clear, without any debris or particles after irradiation by the shaped pulse of 16.2 ps. The energy of each sub-pulse in the shaped pulse of 16.2 ps is small, the surface is gently ablated, and the amount of ejected materials is also very small for each sub-pulse. The ablation dynamics shows that, at a delay time of 3–4 ps after irradiation by a femtosecond laser pulse, the LSFLs appear on a Si surface [25]. Some ejected materials are observed on the surface at a delay time of dozens of picoseconds and will deposit back to the surface [29]. However, under the irradiation of the shaped pulse of 16.2 ps, the ejected materials will be excited by the subsequent sub-pulses, and the plume is further ionized and vaporized, resulting in less deposited debris [29,30].

When the scan velocity decreased to 13 mm/s, continuous, regular, and straight LSFLs are formed on the ablation trace as shown in Fig. 9(c). When the scan velocity decreased to 11 mm/s, the LSFL melted slightly as shown in Fig. 9(d). It is worth noting that, under the irradiation of the shaped pulse of 16.2 ps with such a high laser fluence, although the ripples are partly melted and ablated, no ablation debris is observed on the surface, and the ripples are still very straight.

3. LSFL Fabricated by Temporally Shaped Pulses with Different Intervals

Figure 10 present the confocal optical images of LSFLs fabricated by temporally shaped pulses with different intervals between adjacent sub-pulses. The scanning velocity was 5 mm/s, and the width of each ablation traces was maintained at 26 μm by adjusting the laser fluence. As shown in Fig. 10(a), the LSFLs fabricated by the shaped pulse of 16.2 ps are regularly distributed with a depth of 103 ± 3 nm. As shown in Fig. 10(b), when the sub-pulse interval is reduced to 4.1 ps, the ripples still remain parallel to each other, but the depth decreases significantly to 56 ± 8 nm, and some ripples are partially destroyed. When the interval of the sub-pulses decreases to 1.0 ps, as shown in Fig. 10(c), many visible bifurcations and breakages cause a disarrangement of the ripples. The grooves are very shallow, only 35 nm on an average with a large fluctuation of ±11 nm. When the interval of the sub-pulses is 0.25 ps, the ripples are evidently curved with many bifurcations and breakages as shown in Fig. 10(d). There are even a few deep holes with a depth of approximately 110 nm appearing on the bottom of the ripples.

When the interval of the sub-pulses is less than 1.0 ps, that is, less than the electron-phonon coupling time [25], the temporally shaped pulse will induce an intense thermal accumulation effect rather than an ablation-cooling effect. Thus, the strong thermal hydrodynamics will cause the LSFL to bend and partially submerge. When the interval of sub-pulse increases from 0.25 to 16.2 ps, Fig. 10(e) shows that the period of the LSFL increases from 772 to 793 nm, and the depth increases from 34 to 103 nm. These results show that the period and depth of the LSFL can be well adjusted by a temporally shaped pulse.

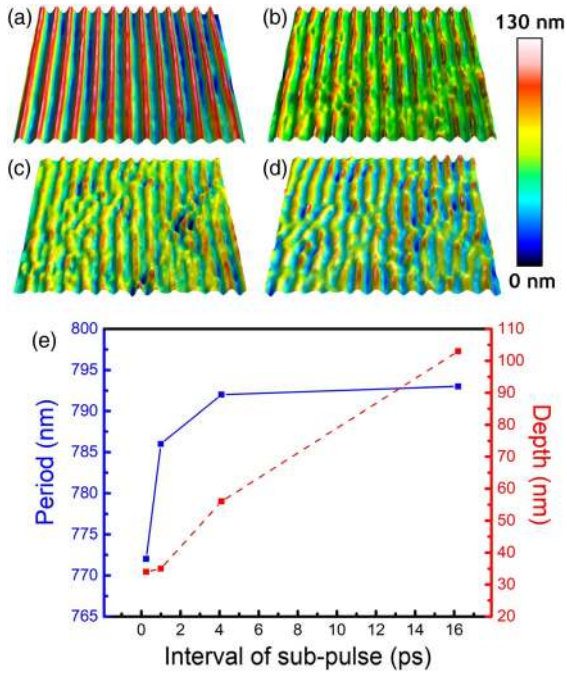

Fig. 10. Confocal optical images of LSFL fabricated by shaped pulse of (a) 16.2 ps, 0.65 J/cm^2; (b) 4.1 ps, 0.44 J/cm^2; (c) 1.0 ps, 0.43 J/cm^2; and (d) 0.25 ps, 0.42 J/cm^2. The scan velocity was fixed as 5 mm/s. (e) The period and depth of the LSFLs for different intervals of sub-pulse.

4. Theoretical Study of the Ultrafast Dynamics of a Si Surface Irradiated by a Temporally Shaped Pulse

When silicon is irradiated by a femtosecond laser pulse with a fluence F, electrons are excited to the conduction band via single-photon absorption, two-photon absorption, free-carrier absorption, and impact ionization. A high-density free carrier N_e is generated on the surface, and the optical properties of Si change from the semiconductor to the metallic state [30,31]. The carriers are rapidly heated by strong electron-electron scattering within tens of femtoseconds [32], and the energy is transferred to the lattice via a carrier-phonon scattering process within several to tens of picoseconds to achieve a thermal equilibrium between electron and lattice systems [32]. To elucidate the mechanism of the formation of LSFL irradiated by a temporally shaped pulse, the evolution of the carrier excitation, the carrier and lattice temperatures, and the transient dielectric constant on the Si surface were studied using the TTM–Drude model [18,25,33]. While numerically solving the TTM–Drude model, the time range was set as −500 to +500 ps with a step size of 1 fs.

Figure 11(a) shows the evolution of the carrier density on the Si surface irradiated by the shaped pulse of 16.2 ps. Because the intensity of the front sub-pulses is weak, the carrier density

increases slowly, and the Auger recombination further reduces the growth rate of the carrier density [33]. When $t = -89.0$ ps, the carrier density gradually increases to 1.0×10^{21} cm^{-3}. Then the intensity of the sub-pulses gradually increases, and the carrier density increases quickly. After irradiation with the two strongest sub-pulses at $t = -8.1$ ps and $t = 8.1$ ps, the carrier density reaches a maximum of 10.3×10^{21} cm^{-3}. Then the carrier density decreases slowly owing to the weakening of the subsequent sub-pulses and the Auger recombination process.

Figure 11(b) shows the evolution of the carrier temperature on the Si surface. The carrier temperature exceeds 10,200 K after the two strongest sub-pulses have arrived at the Si surface. Owing to electron-phonon coupling, the lattice temperature rapidly increases to the melting temperature (1687 K) at $t = 8.3$ ps as shown in Fig. 11(c). The lattice temperature decreases by 40–70 K between two adjacent sub-pulses because of the lattice thermal conductivity [33]. When $t > 150.0$ ps, the lattice temperature reaches a plateau at approximately 2300 K, indicating that the Si surface maintains a mild melting state.

Figure 11(d) shows the evolution of the real part of the dielectric constant ε' of the Si surface. When $t < -56.0$ ps, the real part of the dielectric constant decreases slowly because the electrons are excited by the front weak sub-pulses. When $t = -8.1$ ps, the first strongest sub-pulse reaches the surface, and ε' decreases to −7.88 owing to a high carrier density of 8.05×10^{21} cm^{-3}. The surface changes from a semiconductor to a metal-like state and effectively supports the excitation of SPPs. The subsequent nine sub-pulses can also excite the carrier density to a high level, causing ε' to be less than −1. The width of the temporal envelope for $\varepsilon' < -1$ is 145.8 ps.

The ultrafast dynamics of periodic ripple formation on a Si surface was studied using imaging systems with high spatial-temporal resolution [25,29]. The LSFLs emerge very rapidly, only 3 ps after a single femtosecond laser pulse [25]. This indicates that after irradiation by the strongest sub-pulse at $t = -8.1$ ps, the Si changes from a semiconductor to a metal-like state. When the second strongest sub-pulse ($t = +8.1$ ps) arrives at the surface, the LSFLs appear. These transient ripples enhance the SPPs and lead to a periodic distribution of the laser energy [1]. During the excitation of the SPPs [145.8 ps, as shown in Fig. 11(d)], both melting and ablation can occur [34,35]. Thus, a part of the plasma excited by the strongest pulse is ejected from the surface, removes the deposited heat, and enables ablation cooling [26]. The subsequent sub-pulses further excite the SPPs, enhancing the periodic laser energy deposition. In this case, the SPPs and the periodic laser energy deposition are enhanced, and the residual heat is reduced; thus, clear LSFLs are formed at the center of the ablation spot. Hence, the temporally shaped pulse of 16.2 ps can significantly increase the scan velocity, the window of laser fluence of regular LSFL, and the regularity and LSFL depth.

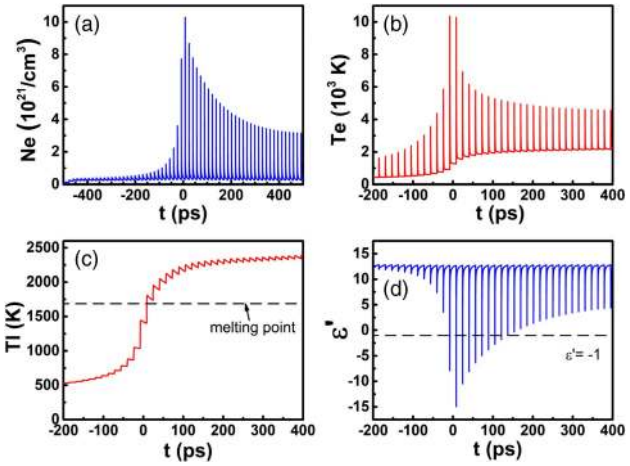

Fig. 11. Evolution of (a) the carrier density, (b) the carrier temperature, (c) the lattice temperature, and (d) the real part of the dielectric constant on the Si surface irradiated with shaped pulse of 16.2 ps.

The theoretically calculated results show that when the Si surface is irradiated by a shaped pulse with an interval less than 1 ps, the width of the temporal envelope of $\varepsilon' < -1$ is less than 10 ps, which means that the excitation of the SPPs lasts for a short time. The interval between two adjacent sub-pulses is less than the time of electron-phonon coupling, and the energy carried away by the lattice heat conduction is very small. Moreover, the lattice temperature only decreases by 0–3 K between two adjacent sub-pulses, and the material ablation is negligible. These results show that when the interval is less than 1 ps, the shaped pulse can enhance the SPPs but to a lesser extent than the shaped pulse of 16.2 ps. Meanwhile, the thermal effect is strong, and the ablation-cooling effect is weak; thus, the regularity of LSFLs is substantially reduced.

4. CONCLUSIONS

In this study, based on a $4f$ configuration zero-dispersion pulse shaping system, an FTL pulse is shaped into a pulse train with varying temporal intervals in the range of 0.25–16.2 ps by periodic π-phase step modulation. The large-area LSFL is efficiently fabricated by the shaped pulse of 16.2 ps by laser direct writing. The grooves of LSFL are very straight with DSOA as low as 2.5°, very uniform with a period of 774 ± 5 nm, and considerably deep with a depth of 97.6 ± 2 nm. The LSFL gratings demonstrate a very bright and pure structural color ranging from blue to red, observed at different angles. The diffraction peaks from 450 to 700 nm are all significantly narrow, only 26 nm on an average, and the diffractive efficiency is 3 times larger than that fabricated by the FTL pulse.

The fabrication efficiency, LSFL depth, and DSOA obtained by using the shaped pulse of 16.2 ps are all considerably better than those by using the FTL pulse. The formation mechanisms of regular LSFLs by using the shaped pulse are experimentally and theoretically studied in detail. The results show that the temporally shaped pulse can enhance the excitation of the SPPs and periodic energy deposition, while reducing the residual thermal effects and the deposition of the ejected debris on the Si surface, eventually resulting in regular and deep LSFL.

Funding. Open Fund of the State Key Laboratory of High Field Laser Physics (Shanghai Institute of Optics and Fine Mechanics); Science and Technology Commission of Shanghai Municipality (19ZR1414500); National Natural Science Foundation of China (11804227, 12074123, 91950112).

Acknowledgment. The English text of this manuscript was edited using the OSA Language Editing Services [36].

Disclosures. The authors declare no conflicts of interest.

REFERENCES

1. M. Huang, F. Zhao, Y. Cheng, N. Xu, and Z. Xu, "Origin of laser-induced near subwavelength ripples: interference between surface plasmons and incident laser," ACS Nano **3**, 4062–4070 (2009).
2. J. Bonse, A. Rosenfeld, and J. Krüger, "On the role of surface plasmon polaritons in the formation of laser-induced periodic surface structures upon irradiation of silicon by femtosecond laser pulses," J. Appl. Phys. **106**, 104910 (2009).
3. T. Q. Jia, H. X. Chen, M. Huang, F. L. Zhao, J. R. Qiu, R. X. Li, Z. Z. Xu, X. K. He, J. Zhang, and H. Kuroda, "Formation of nanogratings on the surface of a ZnSe crystal irradiated by femtosecond laser pulses," Phys. Rev. B **72**, 125429 (2005).
4. A. Y. Vorobyev and C. Guo, "Direct femtosecond laser surface nano/microstructuring and its applications," Laser Photon. Rev. **7**, 385–407 (2013).
5. A. Y. Vorobyev and C. Guo, "Colorizing metals with femtosecond laser pulses," Appl. Phys. Lett. **92**, 041914 (2008).
6. H. Oh, J. Lee, M. Seo, I. U. Baek, J. Y. Byun, and M. Lee, "Laser-induced dewetting of metal thin films for template-free plasmonic color printing," ACS Appl. Mater. Interfaces **10**, 38368–38375 (2018).
7. J. Huang, L. Jiang, X. Li, Q. Wei, Z. Wang, B. Li, L. Huang, A. Wang, Z. Wang, M. Li, L. Qu, and Y. Lu, "Cylindrically focused nonablative femtosecond laser processing of long-range uniform periodic surface structures with tunable diffraction efficiency," Adv. Opt. Mater. **7**, 1900706 (2020).
8. K. Cao, L. Chen, H. Wu, J. Liu, K. Cheng, Y. Li, Y. Xia, C. Feng, S. Zhang, D. Feng, Z. Sun, and T. Jia, "Large-area commercial-grating-quality subwavelength periodic ripples on silicon efficiently fabricated by gentle ablation with femtosecond laser interference via two cylindrical lenses," Opt. Laser Technol. **131**, 106441 (2020).
9. R. Drevinskas, M. Beresna, J. Zhang, A. G. Kazanskii, and P. G. Kazansky, "Ultrafast laser-induced metasurfaces for geometric phase manipulation," Adv. Opt. Mater. **5**, 1600575 (2017).
10. T. Zou, B. Zhao, W. Xin, Y. Wang, B. Wang, X. Zheng, H. Xie, Z. Zhang, J. Yang, and C. Guo, "High-speed femtosecond laser plasmonic lithography and reduction of graphene oxide for anisotropic photoresponse," Light Sci. Appl. **9**, 69 (2020).
11. A. S. Alnaser, S. A. Khan, R. A. Ganeev, and E. Stratakis, "Recent advances in femtosecond laser-induced surface structuring for oil–water separation," Appl. Sci. **9**, 1554 (2019).
12. L. Yong, F. Chen, Q. Yang, Z. Jiang, and X. Hou, "A review of femtosecond-laser-induced underwater superoleophobic surfaces," Adv. Mater. Interfaces **5**, 1701370 (2018).
13. J. E. Sipe, J. F. Young, J. S. Preston, and H. M. van Driel, "Laser-induced periodic surface structure. I. Theory," Phys. Rev. B **27**, 1141–1154 (1983).
14. J. Bonse and S. Graef, "Maxwell meets Marangoni—a review of theories on laser-induced periodic surface structures," Laser Photon. Rev. **14**, 2000215 (2020).
15. L. Jiang, A. Wang, B. Li, T. Cui, and Y. Lu, "Electrons dynamics control by shaping femtosecond laser pulses in micro/nanofabrication: modeling, method, measurement and application," Light Sci. Appl. **7**, 17134 (2017).
16. S. A. Jalil, J. Yang, M. ElKabbash, S. C. Singh, and C. Guo, "Maskless formation of uniform subwavelength periodic surface structures by double temporally-delayed femtosecond laser beams," Appl. Surf. Sci. **471**, 516–520 (2019).
17. J. Huang, L. Jiang, X. Li, A. Wang, Z. Wang, Q. Wang, J. Hu, L. Qu, T. Cui, and Y. Lu, "Fabrication of highly homogeneous and controllable nanogratings on silicon via chemical etching-assisted femtosecond laser modification," Nanophotonics **8**, 869–878 (2019).
18. M. Yang, Q. Wu, Z. Chen, B. Zhang, B. Tang, J. Yao, I. D. Olenik, and J. Xu, "Generation and erasure of femtosecond laser-induced periodic surface structures on nanoparticle-covered silicon by a single laser pulse," Opt. Lett. **39**, 343–346 (2014).
19. K. Cheng, J. Liu, K. Cao, L. Chen, Y. Zhang, Q. Jiang, D. Feng, S. Zhang, Z. Sun, and T. Jia, "Ultrafast dynamics of single-pulse femtosecond laser-induced periodic ripples on the surface of a gold film," Phys. Rev. B **98**, 184106 (2018).
20. K. Cheng, K. Cao, Y. Zhang, R. Han, D. Feng, J. Liu, S. Zhang, Z. Sun, and T. Jia, "Ultrafast dynamics of subwavelength periodic ripples induced by single femtosecond pulse: from noble to common metals," J. Phys. D **53**, 285102 (2020).
21. J. M. Liu, "Simple technique for measurements of pulsed Gaussian-beam spot sizes," Opt. Lett. **7**, 196–198 (1982).
22. A. M. Weiner, D. E. Leaird, G. P. Wiederrecht, and K. A. Nelson, "Femtosecond pulse sequences used for optical manipulation of molecular motion," Science **247**, 1317–1319 (1990).
23. A. M. Weiner, "Femtosecond pulse shaping using spatial light modulators," Rev. Sci. Instrum. **71**, 1929–1960 (2000).
24. A. Lindinger, C. Lupulescu, M. Plewicki, F. Vetter, A. Merli, S. M. Weber, and L. Wöste, "Isotope selective ionization by optimal control using shaped femtosecond laser pulses," Phys. Rev. Lett. **93**, 033001 (2004).
25. J. Liu, X. Jia, W. Wu, K. Cheng, D. Feng, S. Zhang, Z. Sun, and T. Jia, "Ultrafast imaging on the formation of periodic ripples on a Si surface with a prefabricated nanogroove induced by a single femtosecond laser pulse," Opt. Express **26**, 6302–6315 (2018).
26. C. Kerse, H. Kalaycıoğlu, P. Elahi, B. Çetin, D. K. Kesim, Ö. Akçaalan, S. Yavaş, M. D. Aşık, B. Öktem, H. Hoogland, R. Holzwarth, and F. Ö. Ilday, "Ablation-cooled material removal with ultrafast bursts of pulses," Nature **537**, 84–88 (2016).
27. H. Wu, Y. Jiao, C. Zhang, C. Chen, L. Yang, J. Li, J. Ni, Y. Zhang, C. Li, Y. Zhang, S. Jiang, S. Zhu, Y. Hu, D. Wu, and J. Chu, "Large area metal micro-/nano-groove arrays with both structural color and anisotropic wetting fabricated by one-step focused laser interference lithography," Nanoscale **11**, 4803–4810 (2019).
28. J. Schindelin, C. T. Rueden, M. C. Hiner, and K. W. Eliceiri, "The ImageJ ecosystem: an open platform for biomedical image analysis," Mol. Reprod. Dev. **82**, 518–529 (2015).
29. X. Jia, T. Q. Jia, N. N. Peng, D. H. Feng, S. A. Zhang, and Z. R. Sun, "Dynamics of femtosecond laser-induced periodic surface structures on silicon by high spatial and temporal resolution imaging," J. Appl. Phys. **115**, 143102 (2014).
30. K. Sokolowski-Tinten, J. Bialkowski, A. Cavalleri, and D. Linde, "Transient states of matter during short pulse laser ablation," Phys. Rev. Lett. **81**, 224–227 (1998).
31. C. V. Shank, R. Yen, and C. Hirlimann, "Time-resolved reflectivity measurements of femtosecond-optical-pulse-induced phase transitions in silicon," Phys. Rev. Lett. **50**, 454–457 (1983).
32. S. K. Sundaram and E. Mazur, "Inducing and probing non-thermal transitions in semiconductors using femtosecond laser pulses," Nat. Mater. **1**, 217–224 (2002).
33. G. D. Tsibidis, M. Barberoglou, A. Loukakos, E. Stratakis, and C. Fotakis, "Dynamics of ripple formation on silicon surfaces by ultrashort laser pulses in subablation conditions," Phys. Rev. B **86**, 115316 (2012).
34. N. Zhang, X. Zhu, J. Yang, X. Wang, and M. Wang, "Time-resolved shadowgraphs of material ejection in intense femtosecond laser ablation of aluminum," Phys. Rev. Lett. **99**, 167602 (2007).
35. C. Pan, Q. Wang, J. Sun, F. Wang, J. Sun, G. Wang, Y. Lu, and L. Jiang, "Dynamics and its modulation of laser-induced plasma and shockwave in femtosecond double-pulse ablation of silicon," Appl. Phys. Express **13**, 012006 (2020).
36. http://languageediting.osa.org/.